



30th International Conference on Flexible Automation and Intelligent Manufacturing (FAIM2021)
15-18 June 2021, Athens, Greece.

Optimal Sizing of Renewable Microgrid for Flow Shop Systems under Island Operations

Tongdan Jin^a, Vinod Kumar Subramanyam^a, Krystal K. Castillo-Villar^b, Fei Sun^a

^aIngram School of Engineering, Texas State University, San Marcos, TX 78666, USA

^bMechanical Engineering Department/ The Texas Sustainable Energy Research Institute, The University of Texas at San Antonio, San Antonio, TX 78249, USA

* Corresponding author. Tel.: 1-512-245-4904; fax: +1-512-245-7771. E-mail address: tj17@txstate.edu

Abstract

This paper addresses a critical question pertaining to manufacturing sustainability: is it economically viable to implement an island microgrid to power a flow shop system under power demand and supply uncertainty? Though many studies on microgrid sizing are available, the majority assume the microgrid is interconnected with main grid. This paper aims to size wind turbine, photovoltaic and battery storage to energize a multi-stage flow shop system in island mode. A mixed-integer, non-linear programming model is formulated to optimize the renewable portfolio and capacity with the goal of minimizing the levelized cost of energy. The island microgrid is tested in three locations with diverse climate profiles. The results show that net zero energy flow shop production is economically feasible in the areas where the average wind speed exceed 8 m/s at 80-meter tower height, or the battery cost drops below \$100,000/MWh. Sensitivity analyses are further carried out with respect to installation cost, demand response program, production scalability, and weather seasonality.

© 2020 The Authors. Published by Elsevier Ltd.

This is an open access article under the CC BY-NC-ND license (<https://creativecommons.org/licenses/by-nc-nd/4.0/>)

Peer-review under responsibility of the scientific committee of the FAIM 2021.

Keywords: Levelized cost of energy; island microgrid; zero energy building; flow shop scheduling; mixed-integer programming.

1. Introduction

An increasing number of commercial and industrial companies are implementing low-carbon microgrids for self-supply of energy. A microgrid is “a group of interconnected loads and distributed energy resources within clearly defined electrical boundaries that act as a single controllable entity with respect to the grid” [1]. A microgrid can operate in both grid-connected or island mode. Traditional microgrids relied on fossil fuels, but now low-carbon microgrids running with renewable generators become popular, such as wind turbines (WT), solar photovoltaics (PV), and biogas fuel cells.

In literature much attention has been focused on integrating low-carbon microgrids in industrial facilities. At the factory level, Taboada et al. [2] take an early step to size a PV-based microgrid to power a 15 MW wafer fab for minimizing the annualized energy cost. Later on, Villarreal et al. [3] expand the microgrid portfolio by including wind turbine to compensate the PV generation shortage in night. At the production floor,

Moon and Park [4] attempt to minimize the total production cost of a multi-machine, multi-process manufacturing system by combining time-dependent electricity price, energy storage and distributed wind and solar power. These studies show that wind- and solar-based microgrid assist the industrial consumers in achieving self-reliability and security of energy supply as well as the environmental sustainability.

A flow shop manufacturing system, such as an automobile assembly line, refers to the production system where jobs or work-in-processes have the same processing route. Early studies on flow shop scheduling usually focus on performance criteria such as cost, make-span, tardiness, throughput, and release date [5],[6],[7]. Recently much attention is paid to power efficiency, renewable energy integration and environmental sustainability. For instance, Zhang et al. [8] minimize the electricity cost of a grid-tied flow shop system considering on-site solar power generation and battery energy storage (BSS). Biel et al. [9] propose a decision support model for flow shop scheduling with grid-connected onsite wind

power using stochastic mixed-integer linear programming (MILP). Liu et al. [10] investigate an energy-efficient scheduling program for a flexible flow shop that produces and recycles carbon fiber reinforced composite materials. Golpira et al. [11] formulate a risk-based robust mixed-integer linear program to minimize the day-ahead energy cost under peak demand charge. The job shop production system is co-powered by the utility grid and onsite WT, energy storage, and combined heat and power. Khalaf and Wang [12] schedule an energy-cost-aware flow shop considering intermittent renewables, energy storage, and real-time electricity pricing. Wu et al. [13] solve a multi-objective flexible flow shop scheduling problem considering variable job processing time due to variable power supply. These studies show that a renewable microgrid creates multiple benefits, including participating in demand responses, lowering carbon emissions, and improving energy security. A common assumption is that the microgrid is interconnected with the main grid.

Reliable supply of energy is critical to manufacturing in areas of weak grids. The study [14] shows that power outages cost African countries an estimated 1-2% of their annual GDP. Microgrids can help to cope with a lack of reliable grid power supply. Even a highly reliable grid may occasionally have power outages, for example due to extreme weather. During Hurricane Sandy in 2012, the only facilities still running were several microgrids, such as the one at Princeton University [15]. More extreme weather events due to climate change are likely to occur in the decades to come, which stimulates large industrial consumers to implement microgrids.

The paper aims to design an island microgrid system to power flow shop manufacturing systems in a weak grid condition. To the best of our knowledge, few flow shop scheduling models are developed under island microgrid operation. Under load and generation uncertainty, the goal is to jointly optimize renewable portfolio, power capacity and flow shop schedule for minimizing the levelized cost of energy (LCOE). It is defined as the ratio of total generation cost over the annual energy throughput. Energy resources used for constructing the microgrid include WT, PV and BSS units. The novelties of this work include: 1) jointly allocating microgrid capacity and flow shop scheduling, which is often done separately in literature; 2) achieving zero energy performance of manufacturing operations; and 3) capturing the diurnal and seasonal variation of wind and solar generation. The hourly capacity factor in a location is estimated based on 192,720 meteorological data, spanning eleven years from 2006 to 2016.

The remainder of the paper is organized as follows. Section 2 presents a flow shop system with island microgrid. Section 3 formulates a mixed-integer, non-linear programming for sizing renewable microgrid. In Section 4, the flow shop configuration and input parameters of microgrid are provided. Section 5 tests and discusses the proposed model in a variety of climate conditions. Section 6 concludes the work and points the future research direction.

2. A Flow shop system with island microgrid

Fig. 1 shows a flow shop production system connected with a microgrid comprised of WT, PV and BSS. Two operating

scenarios are examined. If the wind blows hard or the sunshine is strong, the facility can be energized by WT and PV with no reliance on BSS. In fact, excess energy is stored in the BSS. When the power of WT and PV is less than the facility's load, the BSS can discharge to co-power the facility. Since the facility is electrically isolated from the main grid, all consumed energy is generated from the renewable microgrid. Hence it naturally attains zero energy performance goal. A zero energy facility, also known net-zero energy building, is a facility with zero net energy consumption, meaning the total amount of energy used by the building on an annual basis is equal to the amount of renewable energy generated on the site [1].

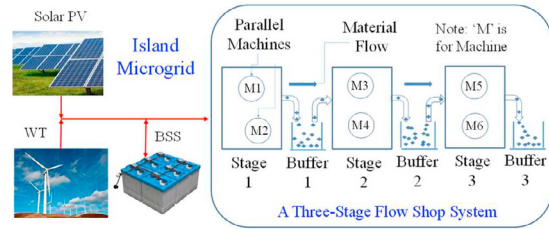


Fig. 1. A flow shop facility powered by island microgrid

3. Optimal microgrid sizing model

We allocate the capacity of WT, PV and BSS to meet the power demand of the flow shop system on hourly basis throughout a year. To facilitate the model presentation, the parameters and decision variables are listed in Table 1.

Table 1. Notation for microgrid sizing model

Parameter	Comments
P_D	: Power demand of the flow shop at time t (unit: MW)
P_{maxCS}	: Maximum power that the battery can be charged
P_{maxDS}	: Maximum power that the battery can discharge
η_{CS}	: Efficiency loss of battery charging
η_{DS}	: Efficiency loss of battery discharging
ϕ_1	: Capital recovery factor of PV system
ϕ_2	: Capital recovery factor of WT system
ϕ_3	: Capital recovery factor of battery system
α_{PV}	: Capacity and operating cost for PV system
α_{WT}	: Capacity and operating cost for WT system
α_B	: Capacity and operating cost for battery system
P_i	: Charging power to the battery at time t
P_o	: Discharging power from the battery at time t
P_{PV}^t	: Power output of PV system at time t , random variable
P_{WT}^t	: Power output of WT system at time t , random variable
P_S^t	: Energy stored in the battery at time t , random variable
CS_t	: Charging status at time t . $CS_t=1$ if the battery is charging, otherwise 0
DS_t	: Discharging status at time t . $DS_t=1$ if the battery is discharging, otherwise 0
λ_{PV}^t	: Capacity factor of PV at time t
λ_{WT}^t	: Capacity factor of WT at time t
$E_{(\infty)}$: Annual energy consumption of the flow shop system, where x is the production schedule (unit: MWh)
Decision Variables:	
P_{PV}^c	: Capacity of the PV system (unit: MW)
P_{WT}^c	: Capacity of the WT system (unit: MW)
P_B^c	: Capacity of the battery (unit: MWh)

Without loss of generality, we assume the planning horizon is one year with $T_p = 8,640$ hours (i.e. $24 \times 7 \times 52$). Denoted as Model SIM or sizing island microgrid, the following mathematical programming is formulated to minimize the levelized cost of energy during the course of a year.

Model SIM (Sizing Island Microgrid):

Minimize:

$$f(P_{PV}^c, P_{WT}^c, P_B^c) = \frac{1}{E(\mathbf{x})} (\phi_1 \alpha_{PV} P_{PV}^c + \phi_2 \alpha_{WT} P_{WT}^c + \phi_3 \alpha_B P_B^c) \tag{1}$$

Subject to:

$$P_{PV}^t + P_{WT}^t - \frac{P_i^t}{\eta_{CS}} + P_o^t \eta_{DS} P_D^t = P^t \quad \text{for } t = 1, 2, \dots, T_p; \tag{2}$$

$$P_{PV}^t = \lambda_{PV}^t P_{PV}^c \quad \text{for } t = 1, 2, \dots, T_p; \tag{3}$$

$$P_{WT}^t = \lambda_{WT}^t P_{WT}^c \quad \text{for } t = 1, 2, \dots, T_p; \tag{4}$$

$$0 \leq P_S^t \leq P_B^c \quad \text{for } t = 1, 2, \dots, T_p; \tag{5}$$

$$P_i^t \leq P \max_{CS} CS_i \quad \text{for } t = 1, 2, \dots, T_p; \tag{6}$$

$$P_o^t \leq P \max_{DS} DS_i \quad \text{for } t = 1, 2, \dots, T_p; \tag{7}$$

$$P_S^t - P_S^{t-1} = P_o^t - P_i^t \quad \text{for } t = 1, 2, \dots, T_p; \tag{8}$$

$$CS_i + DS_i \leq 1 \quad \text{for } t = 1, 2, \dots, T_p; \tag{9}$$

$$CS_i, DS_i \in \{0, 1\} \quad \text{for } t = 1, 2, \dots, T_p; \tag{10}$$

$$P_{PV}^c, P_{WT}^c, P_B^c \geq 0 \quad \text{for } t = 1, 2, \dots, T_p; \tag{11}$$

The objective function (1) aims to minimize the LCOE where the denominator represents the total energy use of the flow shop in period T_p , which is obtained from the flow shop scheduling model in [8],[16], and the numerator represents the annualized cost of the flow shop system. The annualized cost consists of the investment and operating cost of WT, PV, and BSS. Since the planning horizon is one year, ϕ_1 , ϕ_2 , and ϕ_3 represent the capital recovery factor of PV, WT, and BSS, respectively. Constraints (2) shows that the total energy drawn from PV, WT, and BSS is equal to the demand of the flow shop at each operation period. This hourly demand is obtained from solving the model in [8]. Constraints (3) and (4) define the actual output power of PV and WT at time t based on the capacity factor. Constraint (5) states that the maximum amount of stored energy in BSS should not exceed its capacity limit. Constraints (6) and (7) define the maximum energy that can be charged or discharged at time t . Constraint (8) states that the net energy of BSS between $t-1$ and t equals the sum of charged and discharged energy in that period. Constraint (9) ensures that battery charge and discharge cannot occur at the same time. Constraints (10) and (11) define the non-negativity of all the decision variables.

Model 1 is coded with the AMPL programming language and solved using the CPLEX search engine. The algorithm runs in an Intel(R) Core (TM) i7-8550U processor with 1.8 GHz 1.99 GHz, and 12 GB DRAM. The current model has a total of three decision variables and 77,760 constraints. As we are solving Model 1 on an hourly basis, the power demand in each time-period is equal to the energy use per period.

4. Experimental Settings

4.1. Climate data of testing cities

Three cities with diverse wind and weather conditions are chosen to test Model SIM. They are Wellington in New Zealand, Aswan in Egypt, and San Francisco in California of the USA. For each city, hourly wind speed and weather state between 2006 and 2016 are retrieved from the Weather

Underground portal [17], and used to estimate the capacity factor. Table 2 summarizes the annual climate conditions of these cities. Wellington has a strong wind profile with less sunshine, Aswan has extreme sunshine but weak wind, and San Francisco possesses medium wind and sunshine condition. Note 80 m is the typical tower height of modern wind turbines.

Table 2. Wind speed at 80 m tower height and weather states.

Feature	Cities	Wellington	Aswan	San Francisco
Wind (m/s)	Average speed	13.61	5.93	8.21
	Std. deviation	4.08	1.78	2.46
Weather state (day)	Clear sky	6	356	28
	Scattered cloud	68	5	95
	Partially cloudy	109	3	136
	Mostly cloudy	5	0	13
	Overcast	1	0	2
	Rain	170	0	65
	Fog	2	0	24
	Storm/T-storm	3	0	3
Climate Profile	Wind speed	High	Low	Medium
	Sunshine	Low	High	Medium

4.2. Electric load of flow shop system

A three-stage hybrid flow shop system with parallel machines shown in Fig. 1 is used to demonstrate the application of Model SIM. Table 3 presents power demand and processing time of individual jobs which are related to wafer fabrication running in 24/7 mode. Without loss of generality, the baseload of the flow shop is assumed to be 1 MW for keeping the lights on as well as running basic air ventilation equipment.

Table 3. Job processing power and time at different stages.

Job, stage, machines	Power use (MW)	Processing time (hour/job)	{Job, stage, machines}	Power use (MW)	Processing time (hour/job)
{1, 1, 1}	3	40	{2, 1, 1}	4	40
{1, 1, 2}	4	40	{2, 1, 2}	3	40
{1, 1, 3}	4	40	{2, 1, 3}	4	40
{1, 2, 1}	3	60	{2, 2, 1}	4	60
{1, 2, 2}	3	60	{2, 2, 2}	5	60
{1, 2, 3}	4	60	{2, 2, 3}	4	60
{1, 3, 1}	3	40	{2, 3, 1}	3	40
{1, 3, 2}	4	40	{2, 3, 2}	4	40
{1, 3, 3}	4	40	{2, 3, 3}	4	40

Table 4. Job throughput requirement from January to December.

Month	1	2	3	4	5	6	7	8	9	10	11	12
Job 1	4	4	5	5	5	6	6	7	7	6	5	4
Job 2	4	4	5	5	5	6	6	7	7	6	5	4

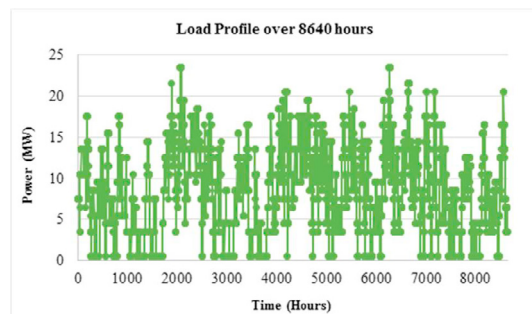


Fig. 2. Power demand of the flow shop system [16]

There are two jobs being processed concurrently, and Table 4 defines the job throughput requirement from January to December of a year. The power scheduling model in [16]

allocates the production schedule of Jobs 1 and 2 to meet the required throughput with minimum energy consumed across a year. There are two parallel machines in each stage. The buffer size of stages 1 and 2 is five, and the buffer capacity in the last stage is unlimited. The resulting power demand curve is plotted in Fig. 2. By summing the hourly demand, the annual energy use reaches $E(x)=75,928.5$ MWh.

4.3. Cost parameter of microgrid components

Table 5 lists the input parameters for Model SIM. Though the cost of WT, PV and BSS may vary, the values presented in the table are based on the NREL reports [18],[19],[20]. O&M stands for operation and maintenance.

Table 5. Cost and Related Parameters of WT, PV and BSS

Notation	Value	Comment
α_{PV}	\$3.0M/MW	PV capacity cost including O&M expense
α_{WT}	\$1.5M/MW	WT capacity cost including O&M expense
α_{BS}	\$0.5M/MWh	BSS capacity cost including O&M expense
ϕ_{PV}	0.0802	PV with 20-year lifetime, 5% discount rate
ϕ_{WT}	0.0802	WT with 20-year lifetime, 5% discount rate
ϕ_{BS}	0.1295	BS with 10-year life, and 5% discount rate
η_{CS}	0.9	Battery charging efficiency
η_{DS}	0.9	Battery discharging efficiency

5. Results and discussion

In this section, Model SIM is solved using the power demand curve in Fig. 2. For each city the model is solved in four difference cases shown in Table 6. Case 1 is the benchmark case. Cases 2 and 4 are used for sensitivity analysis, and the cost of PV and WT changes and declines to reflect the down trend as the technology advances. In each case, the BSS cost varies from 0.5 to \$0.01M/MWh. For each city, we compare the LCOE and capacity of WT, PV and BSS in difference cases.

Table 6. Four design cases for each city (Case 1 is the benchmark).

Case	WT Cost (\$M/MW)	PV Cost (\$M/MW)	BSS Cost (\$M/MWh)
1	1.5	3	0.5 to 0.01
2	1.5	1.5	0.5 to 0.01
3	1	1	0.5 to 0.01
4	1	0.5	0.5 to 0.01

5.1. Wellington

Fig. 4 graphically shows the results of four cases in Wellington. A common observation is that PV is not competitive in all cases even if its cost is down to \$0.5M/MW. This result is not surprising because the average wind speed in Wellington is 13.61 m/s with only six clear days per year. Another interesting observation is that LCOE decreases with the BSS size. Fig. 3 represents the outcome of Case 1, showing the required WT capacity is 40.5 MW in order to meet the annual energy use of the flow shop system. There is no BSS installation if its cost falls in a range between 0.1 and \$0.5M/MWh; However, BSS becomes preferable if its cost is down below \$0.1M/MWh. Using BSS also reduces the LCOE from \$64/MWh to \$45/MWh if more BSS capacity is installed. Case 2 in Fig. 4 simply shows that the renewable portfolio and capacity of the microgrid remain unchanged even if the PV cost is cut off by 50%. Cases 3 and 4 (see Fig. 5 and 6) shows that if the WT cost is down to \$1M/MW, the LCOE reduces to \$43/MWh which is expected, but the BSS is also becomes less competitive.

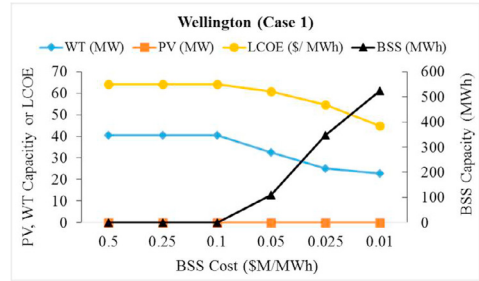


Fig. 3. Microgrid capacity and LCOE in Wellington for Case 1

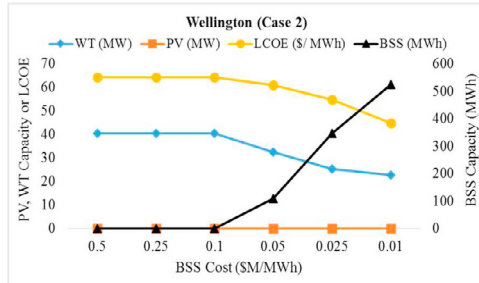


Fig. 4. Microgrid capacity and LCOE in Wellington for Case 2

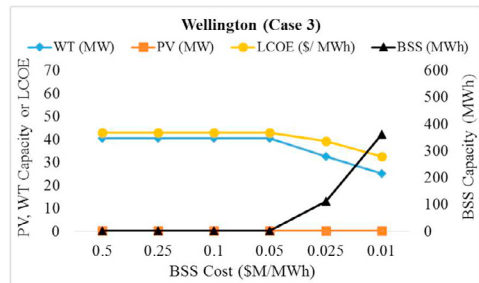


Fig. 5. Microgrid capacity and LCOE in Wellington for Case 3

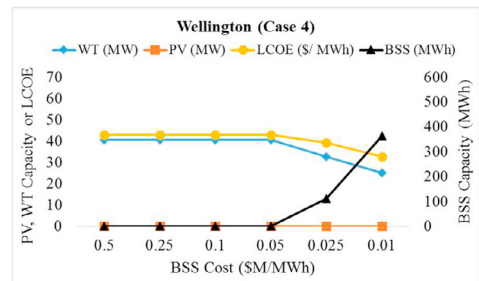


Fig. 6. Microgrid capacity and LCOE in Wellington for Case 4

5.2. Aswan

Case 1 in Fig. 7 is the benchmark case for Aswan, and the microgrid chooses to install wind capacity of 122 MW at a minimum LCOE of \$194/MWh. The reason is due to the unavailability of the PV generation during night times. Thus, an island microgrid in Aswan does not consider any PV even if there are 356 clear days. Battery capacity of 8.3 MWh, 62.97 MWh and 264.13 MWh is installed corresponding to the capacity cost of 0.5, 0.25 and \$0.1M/MWh, respectively.

In Case 2 of Fig. 8, the PV cost is down to \$1.5M/MW, the

island system start to penetrate 20 MW PV while the WT capacity is reduced to an average of 88 MW. At the meantime, the BSS installation increases with the PV size. This is expected because PV has no output in the night, and the BSS serves as the complementary energy source.

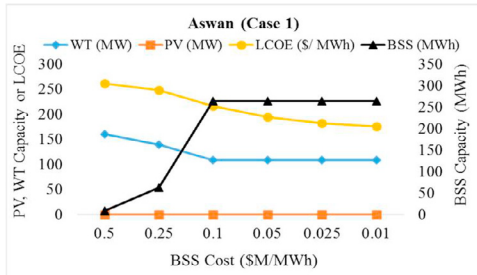


Fig. 7. Microgrid capacity and LCOE in Aswan for Case 1

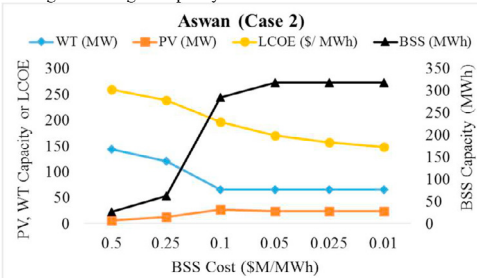


Fig. 8. Microgrid capacity and LCOE in Aswan for Case 2

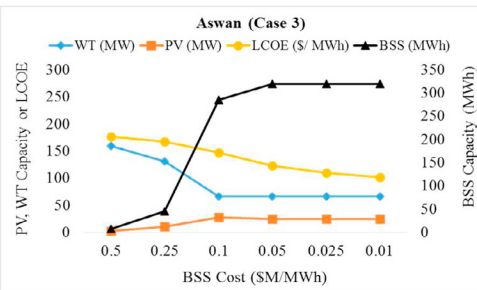


Fig. 9. Microgrid capacity and LCOE in Aswan for Case 3

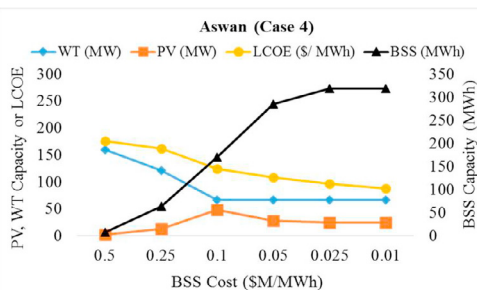


Fig. 10. Microgrid capacity and LCOE in Aswan for Case 4

In Case 3 of Fig. 9, the capacity cost of PV and WT equals \$1M/MW, the microgrid system tends to incorporate both wind and solar generation, the PV installation increases with the battery capacity costs down from \$0.5M/MWh to 0.1M/MWh. However, the PV capacity is saturated when the BSS cost drops below 0.1M/MWh. In Case 4 (see Fig. 10), we further reduce the PV cost to \$0.5M/MW. The PV and BSS installation

increases, and WT capacity decreases when BSS cost is between \$0.25M/MWh and 0.5M/MWh. At battery cost of \$0.1M/MWh, the PV capacity reaches the peak of 48.16 MW and then starts to decline with the BSS cost.

5.3. San Francisco

San Francisco has medium wind and sunshine conditions. The average wind speed is 8.21 m/s, and the number of clear, scattered cloud and partially cloudy days is 28, 95, and 136, respectively, together accounting for 70% of time of a year. Fig. 11 to 14 depicts the sizing and LCOE of four cases in San Francisco. A common observation is that wind generation dominates the microgrid power while PV becomes competitive only if the cost is down to \$0.5M/MW. Another interesting observation is that BSS is also preferred even if its cost is as high as \$0.5M/MWh as shown in Cases 1 and 2. In Cases 3 and 4 where the WT cost is only \$1M/MW, the BSS is a still a desirable source for the microgrid as long as its cost is below \$0.5M/MWh. In Cases 1 and 2, the LCOE varies from \$150/MWh to \$225/MWh depending on the BSS size. In Cases 3 and 4, the LCOE falls in a range between \$100/MWh and \$149/MWh. It drops because of reduced PV and WT cost.

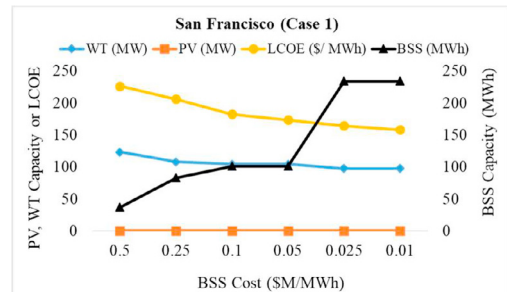


Fig. 11. Microgrid capacity and LCOE in San Francisco for Case 1

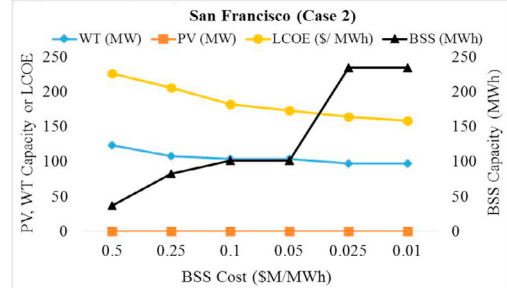


Fig. 12. Microgrid capacity and LCOE in San Francisco for Case 2

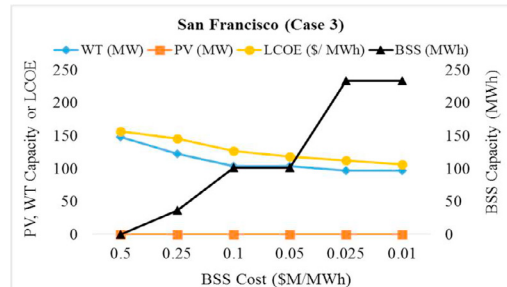


Fig. 13. Microgrid capacity and LCOE in San Francisco for Case 3

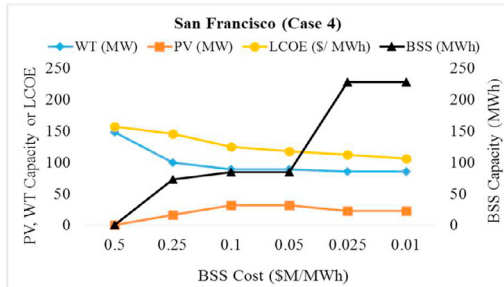


Fig. 14. Microgrid capacity and LCOE in San Francisco for Case 4

6. Conclusion

In this paper a mixed-integer non-linear optimization model is formulated to allocate the capacity of island microgrid in a flow shop manufacturing setting. The objective is to minimize the levelized cost of energy, and this is achieved by optimizing the size of wind turbine, solar panels and battery storage units subject to uncertain climate conditions. The microgrid sizing model is tested in Wellington, Aswan and San Francisco with a broad range of climate conditions. Three insights are derived from the numerical experiments. First, in island mode wind generation at speed of 6 m/s is still competitive even in locations where the number of clear sky days exceeds 95% time of a year. Second, photovoltaics and battery systems can only compete with wind power if their costs are down to \$1.5M/MWh and \$0.25M/MWh, respectively. Third, in a location with medium wind and sunshine, an energy mix of wind and battery turns out to be more cost-effective despite the current high cost of the battery technology. In future research, this work can be expanded by considering a multi-building environment for the optimization of both flow shop scheduling and energy exchange model. The current model can also be extended to production systems with re-entrant jobs instead of feed forward production.

Acknowledgements

This project is supported by NSF CBET Program (#1704933).

References

- [1] US DOE. A common definition for zero energy buildings. US Department of Energy (DOE) report. 2015. Available at <https://www.energy.gov/eere/buildings>, (accessed on Oct., 2, 2019).
- [2] Taboada H., Xiong Z., Jin T, Jimenez JA. Exploring a solar photovoltaic-based energy solution for a green manufacturing environment. In Proceedings of IEEE Conference on Automation Science and Engineering, 2012, pp. 40-45.
- [3] Villarreal S, Jimenez JA, Jin T, Cabrera-Rios M. Designing a sustainable and distributed generation system for semiconductor wafer fabs. IEEE Transactions on Automation Science and Engineering, 2013, 10(1), pp. 16-26.
- [4] Moon J-Y, Park J. Smart production scheduling with time-dependent and machine-dependent electricity cost by considering distributed energy resources and energy storage. International Journal of Production Research, 2014, 52(13), pp. 3922-3939.
- [5] Ruiz R, Vázquez-Rodríguez JA. The hybrid flow shop scheduling problem. European Journal of Operational Research. 2010, 205(1), pp. 1-18.
- [6] Yenisey MM, Yagmahan B. Multi-objective permutation flow shop scheduling problem: Literature review, classification and current trends. Omega, 2014, 45(6), pp. 119-135.
- [7] May G, Stahl B, Taisch M, Prabhu V. Multi-objective genetic algorithm for energy-efficient job shop scheduling. International Journal of Production Research, 2015, 53(23), pp. 7071-7089.
- [8] Zhang H, Cai J, Fang K, Zhao F, Sutherland JW. Operational optimization of a grid-connected factory with onsite photovoltaic and battery storage systems. Applied Energy, 2017, 205, pp.1538-1547.
- [9] Biel K, Zhao F, Sutherland JW, Glock CH. Flow shop scheduling with grid-integrated onsite wind power using stochastic MILP. International Journal of Production Research, 2018, 56(5), pp. 2076-2098
- [10] Liu Y, Farnsworth M, Tiwari A. Energy-efficient scheduling of flexible flow shop of composite recycling. The International Journal of Advanced Manufacturing Technology, 2018, 97(1-4), pp. 117-127.
- [11] Golpîra H, Khan SAR, Zhang Y. Robust smart energy efficient production planning for a general job-shop manufacturing system under combined demand and supply uncertainty in the presence of grid-connected microgrid. Journal of Cleaner Production, 2018, 202, pp. 649-665.
- [12] Khalaf AF., Wang Y. Energy-cost-aware flow shop scheduling considering intermittent renewables, energy storage, and real-time electricity pricing. International Journal of Energy Research, 2018, 42, pp. 3928-3942.
- [13] Wu X, Shen X., Cui Q. Multi-objective flexible flow shop scheduling problem considering variable processing time due to renewable energy. Sustainability. 2018, 10(3), pp. 1-30 (<https://doi.org/10.3390/su10030841>).
- [14] CDC Group. What are the links between power, economic growth and job creation?. 2016 available at <http://www.cdcgroup.com/Documents/>. (accessed on July 3, 2019).
- [15] Greentech Media. How microgrids helped weather Hurricane Sandy. 2012, available at <https://www.greentechmedia.com/articles>. (Accessed on August 20, 2019).
- [16] Subramanyam VK. Designing multi-period production and flow shop manufacturing systems with island microgrid operation. Master Thesis, 2018, Texas State University. available at <https://digital.library.txstate.edu/handle/10877/7882>. (accessed on November 5, 2019).
- [17] WU. Weather Underground Portal. 2018, available at <http://www.wunderground.com/>, (accessed August 2, 2018).
- [18] Fu R, Feldman D, Margolis R, Woodhouse M, Ardani K. The U.S. solar photovoltaic system cost benchmark: Q1 2017. National Renewable Energy Laboratory Report. 2018, Available at <https://www.nrel.gov/docs/fy17osti/68925.pdf>. (accessed on September 21, 2019).
- [19] Stehly TJ, Beiter PC, Heimiller DM, Scott GN. 2017 cost of wind energy review. National Renewable Energy Lab Report, 2018. Available at <https://www.nrel.gov/docs/fy18osti/72167.pdf>. (accessed on September 21, 2019).
- [20] Fu R, Remo T, Margooslis R. The 2018 U.S. utility-scale photovoltaics-plus-energy storage system costs benchmark. National Renewable Energy Laboratory Report. 2018. Available at <https://www.nrel.gov/docs/fy19osti/71714.pdf>. (accessed on September 21, 2019).